

Channeling in direct dark matter detection II : channeling fraction in Si and Ge crystals

Nassim Bozorgnia

*Department of Physics and Astronomy, UCLA, 475 Portola Plaza, Los Angeles, CA
90095, USA*

E-mail: nassim@physics.ucla.edu

Graciela B. Gelmini

*Department of Physics and Astronomy, UCLA, 475 Portola Plaza, Los Angeles, CA
90095, USA*

Email: gelmini@physics.ucla.edu

Paolo Gondolo

*Department of Physics and Astronomy, University of Utah, 115 South 1400 East #201,
Salt Lake City, UT 84112, USA*

School of Physics, KIAS, Seoul 130-722, Korea

E-mail: paolo@physics.utah.edu

ABSTRACT: The channeling of the ion recoiling after a collision with a WIMP changes the ionization signal in direct detection experiments, producing a larger signal than otherwise expected. We give estimates of the fraction of channeled recoiling ions in Si and Ge crystals using analytic models produced since the 1960's and 70's to describe channeling and blocking effects. We used data obtained to avoid channeling in the implantation of dopants in Si crystals to test our models.

Contents

1. Introduction	1
2. Model of Channeling	2
2.1 Continuum models	2
2.2 The transverse energy	5
2.3 Minimum distances of approach and critical channeling angles	6
2.4 Temperature dependent critical distances and angles	12
3. Channeling of recoiling lattice nuclei	17
3.1 Channeling fraction for each channel	17
3.2 Total geometric channeling fraction	19
4. Main results and conclusions	20
Appendices	23
A. Penetration length of channeled ions	23
B. Crystal structure of Si and Ge	25
C. Probability of correlated channels	26

1. Introduction

Channeling and blocking effects in crystals refer to the orientation dependence of charged ion penetration in crystals. In the “channeling effect” ions incident upon a crystal along symmetry axes and planes suffer a series of small-angle scatterings that maintain them in the open “channels” in between the rows or planes of lattice atoms and thus penetrate much further into the crystal than in other directions. Channeled incident ions do not get close to lattice sites, where they would be deflected at large angles.

The “blocking effect” consists in a reduction of the flux of ions originating in lattice sites along symmetry axes and planes, due to large-angle scattering with the atoms immediately in front of the originating lattice site, creating what is called a “blocking dip” in the flux of ions exiting from a thin enough crystal as function of the exit angle with respect to a particular symmetry axis or plane.

Channeling and blocking effects in crystals are related because the non-channeled incident ions are those which suffer a close-encounter process with an atomic nucleus in the crystal, namely those which pass sufficiently close to a lattice nucleus to be deflected at a large angle. After a close-encounter collision the deflected ion acts as if it was “emitted” from a lattice site. Channeling is many times observed as a lack of ions (incident at a small angle ψ with respect to a particular symmetry axis or plane) deflected at a large-angle which form a “channeling dip” in the outgoing flux as function of the incident beam angle ψ . As pointed out first by Lindhard [1], when no slowing-down processes are involved the “channeling” and “blocking” dips should be identical, when compared for the same particles, energies, crystals and crystal directions.

Channeled ions lose their energy to electrons. They penetrate distances much larger than the characteristic separation of atoms along the channels, thus they interact with hundreds or thousands of lattice atoms. For energies in the keV range and above, channeled ions penetrate distances of at least several 10’s of nm (see Appendix A, where we use the Lindhard-Scharff [2, 3] model of electronic energy loss to calculate the penetration length of ions). These are distances much longer than the separation of atoms along the channels, which are similar to the lattice constant, i.e. approximately 0.5 nm for Si and Ge (see Appendix B).

The potential importance of the channeling effect for direct dark matter detection was first pointed out for NaI (Tl) by Drobyshovski [4] and by the DAMA collaboration [5]. The prospect of a daily modulation of the dark matter signal in direct detection due to channeling was recently raised by Avignone, Creswick and Nussinov [6] in NaI.

In this paper we compute the channeling fraction of recoiling ions in Si and Ge crystals as function of the recoil energy and temperature. Si and Ge crystals are used in several direct dark matter detection experiments, such as CDMS [7], CoGeNT [8], Edelweiss [9], TEXONO [10], EURECA [11], HDMS [12] and IGEX [13]. In a companion paper [14] we introduced the general ideas and analytic models [1, 3, 15, 16, 17, 18, 19, 20, 21, 22] that we use to describe these phenomena in the context of dark matter detection, and applied them to NaI (Tl). For the reader familiar with Ref. [14] we would like to clarify which are the main differences between the calculations in Ref. [14] and in the present paper, besides the crystal structure (see Appendix B). In this paper we use a different expression for the continuum potentials (see Eqs. 2.1 to 2.7), which leads to a different expression for the critical channeling distance for axial channels (see Eq. 2.15). We also use a different way of deriving the critical distance for planar channels (see Eqs. 2.18 to 2.23).

2. Model of Channeling

2.1 Continuum models

There are different approaches to calculate the deflections of ions traveling in a crystal. In “binary collision models” the ion path is computed by a computer program (see Ref. [23] for one of the first ones) in terms of a succession of individual interactions, each with one of the atoms in the crystal. Crystal imperfections and lattice vibrations are thus easily and

correctly taken into account. In “continuum models”, reasonable approximations are made which allow to replace the discrete series of binary collisions with atoms by a continuous interaction between a projectile and uniformly charged strings or planes. These models allow to replace the numerical calculations by an analytic description of channeling, and provide good quantitative predictions of the behavior of projectiles in the crystal in terms of simple physical quantities. This is the approach we use here.

The analytical description of channeling phenomena was initially developed mostly by J. Lindhard [1] and collaborators for ions of energy MeV and higher, and its use was later extended to lower energies, i.e. hundreds of eV and above, mostly to apply it to ion implantation in Si. For the low energy range, we found most useful the work of G. Hobler [22], who in 1995 and 1996 perfected and checked experimentally previous continuum model predictions [24] for axial and planar channeling at energies in the keV to a few 100 keV range, developed to avoid channeling in the implantation of B, P and As atoms in Si crystals [25]. This approach must be complemented by determination of parameters through data fitting or simulations. Moreover, lattice vibrations are more difficult to include in continuum models. Since we use a continuum model, our results should in last instance be checked by using some of the many sophisticated simulation programs that implement the binary collision approach or mixed approaches (e.g. [26]).

Our calculation is based on the classical analytic models developed in the 1960’s and 70’s, in particular by Lindhard [1, 3, 16, 17, 18, 19, 20, 21, 22]. The fact that the de Broglie wavelengths of ions in the keV energy range are of the order of ~ 0.01 pm (and smaller at higher energies), thus much shorter than the lattice constant of a crystal (~ 500 pm, see Appendix B), justifies using a classical treatment. We use the continuum string and plane model, in which the screened Thomas-Fermi potential is averaged over a direction parallel to a row or a plane. This averaged potential is considered to be uniformly smeared out along the row or plane of atoms, which is a good approximation if the propagating ion interacts with many lattice atoms in the row or plane by a correlated series of many consecutive glancing collisions with lattice atoms. We are going to consider just one row, which simplifies the calculations and is correct except at the lowest energies we consider, as we explain below.

There are several good analytic approximations of the screened potential. Except when said otherwise, in this paper we use Molière’s approximation, following the work of Hobler [22] and Morgan and Van Vliet [17, 18]. Molière’s approximations of the continuum potentials are more complicated and also somewhat better than Lindhard’s expressions, which we used in our paper devoted to NaI [14]. Lindhard’s expressions are easier to manipulate algebraically to obtain different quantities of interest. Still in this paper we used some expressions derived from Lindhard’s form of the potentials.

In Molière’s approximation [15] the axial continuum potential, as a function of the transverse distance r to the string, is

$$U(r) = (2Z_1Z_2e^2/d) f(r/a) = E\psi_1^2 f(r/a), \quad (2.1)$$

where E is the energy of the propagating particle and ψ_1 is a dimensionless parameter defined

by

$$\psi_1^2 = \frac{2Z_1Z_2e^2}{Ed}, \quad (2.2)$$

Z_1, Z_2 are the atomic numbers of the recoiling and lattice nuclei respectively, d is the spacing between atoms in the row, a is the Thomas-Fermi screening distance, $a = 0.4685\text{\AA}(Z_1^{1/2} + Z_2^{1/2})^{-2/3}$ [23, 15] (1.225×10^{-2} nm and 0.9296×10^{-2} nm for a Si ion in Si and a Ge ion in Ge respectively, see Appendix B) and $E = Mv^2/2$ is the kinetic energy of the propagating ion. Molière's screening function [15] for the continuum potential is

$$f(\xi) = \sum_{i=1}^3 \alpha_i K_0(\beta_i \xi). \quad (2.3)$$

Here K_0 is the zero-order modified Bessel function of the second kind, and the dimensionless coefficients α_i and β_i are $\alpha_i = \{0.1, 0.55, 0.35\}$ and $\beta_i = \{6.0, 1.2, 0.3\}$ [27], for $i = 1, 2, 3$. The string of crystal atoms is at $r = 0$.

In our case, E is the recoil energy imparted to the ion in a collision with a WIMP,

$$E = \frac{|\vec{\mathbf{q}}|^2}{2M}, \quad (2.4)$$

and $\vec{\mathbf{q}}$ is the recoil momentum.

The continuum planar potential in Molière's approximation [15], as a function of the distance x perpendicular to the plane, is

$$U_p(x) = (2\pi n Z_1 Z_2 e^2 a) f_p(x/a) = E \psi_a^2 f_p(x/a), \quad (2.5)$$

where the dimensionless parameter ψ_a is defined as

$$\psi_a^2 = \frac{2\pi n Z_1 Z_2 e^2 a}{E}, \quad (2.6)$$

and $n = Nd_{pch}$ is the average number of atoms per unit area, where N is the atomic density and d_{pch} is the width of the planar channel, i.e. the interplanar spacing (thus, the average distance of atoms within a plane is $d_p = 1/\sqrt{Nd_{pch}}$). The subscript p denotes ‘‘planar’’ and

$$f_p(\xi) = \sum_{i=1}^3 (\alpha_i/\beta_i) \exp(-\beta_i \xi), \quad (2.7)$$

where the coefficients α_i and β_i are the same as above. The plane is at $x = 0$.

Examples of axial and planar continuum potentials for a Si ion propagating in a Si crystal and a Ge ion propagating in a Ge crystal are shown in Fig. 1.

The continuum model does not imply that the potential energy of an ion moving near an atomic row is well approximated by the continuum potential U . The actual potential consists of sharp peaks near the atoms and deep valleys in between. The continuum model says that the net deflection due to the succession of impulses from the peaks is identical to

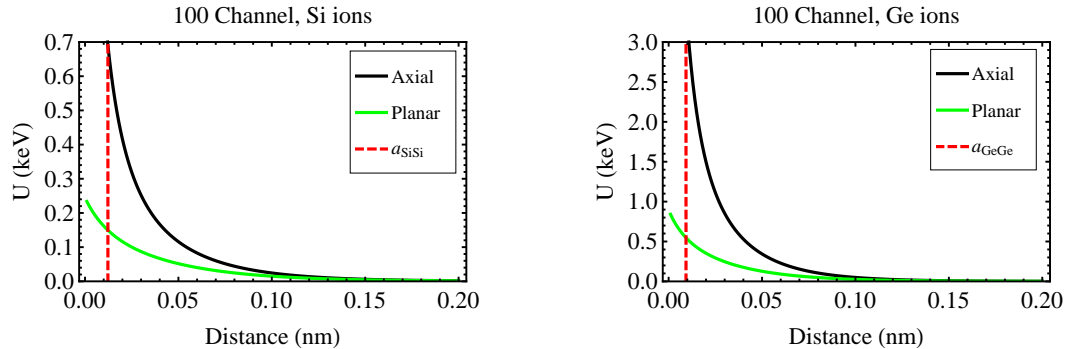


Figure 1: Continuum axial (black) and planar (green/gray) potentials for (a) Si and (b) Ge ions, propagating in the $\langle 100 \rangle$ axial and $\{100\}$ planar channels of a Si or Ge crystal respectively. The screening radii shown as vertical lines are $a_{SiSi} = 0.01225$ nm and $a_{GeGe} = 0.009296$ nm (see Appendix B).

the deflection due to a force $-U'$. This is only so if the ion never approaches so closely any individual atom that it suffers a large-angle collision. Lindhard proved that for a string of atoms this is so only if

$$U''(r) < \frac{8}{d^2} E, \quad (2.8)$$

where the double prime denotes the second derivative with respect to r . Replacing the inequality in Eq. 2.8 by an equality defines an energy dependent critical distance r_c such that $r > r_c$ for the continuum model to be valid. Morgan and Van Vliet [17] also derived a condition for axial channels, similar to Eq. 2.8 but with the factor 8 replaced by 16.

The breakdown of the continuum theory for a planar channel is more involved than for an axial channel because the atoms in the plane contributing to the scattering of the propagating ion are usually displaced laterally within the plane with respect to the ion's trajectory. Thus the moving ion does not encounter atoms at a fixed separation or at fixed impact parameter as is the case for a row. Morgan and Van Vliet [17] reduced the problem of scattering from a plane of atoms to the scattering of an equivalent row of atoms contained in a strip centered on the projection of the ion path on the plane of atoms. They then applied Eq. 2.8 as the condition for planar channeling to the fictitious string defined in this way (more about this below).

2.2 The transverse energy

Lindhard proved that for channeled particles the longitudinal component $v \cos \phi$ of the velocity, i.e. the component along the direction of the row or plane of the velocity, may be treated as constant (if energy loss processes are neglected). Then, in the continuum model, the trajectory of the ions can be completely described in terms of the transverse direction, perpendicular to the row or plane considered. For small angle ϕ between the ion's trajectory and the atomic row (or plane) in the direction perpendicular to the row (or plane), the so

called “transverse energy”

$$E_{\perp} = E \sin^2 \phi + U \simeq E\phi^2 + U \quad (2.9)$$

is conserved. In Eq. 2.9 relativistic corrections are neglected.

Let r_i be the initial position at which the WIMP nucleus collision occurs, i.e. if $r_i > 0$ the recoiling nucleus was displaced with respect to its position of equilibrium in a crystal row when it collided with a WIMP. We call ϕ_i the angle of the initial recoil momentum with respect to the row of atoms and E the initial recoil energy of the propagating ion. Given these initial parameters, the issue of where to define E_{\perp} arises. Namely, we define

$$E_{\perp} = E \sin^2 \phi_i + U(r^*), \quad (2.10)$$

but there are different possible choices for r^* , the position at which to measure the potential U . In our case, the recoiling ion leaves an empty lattice site, thus it moves away from an empty lattice site in the potential generated by its neighboring lattice atoms. So the potential the recoiling ion moves through at the moment of collision is very small, and the recoiling ion conserves its momentum and direction of motion until it gets very near the nearest neighbor, a distance d away along the string. At this moment, it is at a distance

$$r^* \equiv r_i + d \tan \phi_i \quad (2.11)$$

from its nearest neighbor. Therefore, as we did in Ref. [14], we will make the approximation of defining the potential entering into Eq. 2.10 at this position r^* .

2.3 Minimum distances of approach and critical channeling angles

The conservation of the transverse energy provides a definition of the minimum distance of approach to the string, r_{\min} (or to the plane of atoms x_{\min}), at which the trajectory of the ion makes a zero angle with the string (or plane), and also of the angle ψ at which the ion exits from the string (or plane), i.e. far away from it where $U \simeq 0$. In reality the furthest position from a string or plane of atoms is the middle of the channel, whose width we call d_{ach} for an axial channel (d_{pch} for a planar channel). Thus, for an axial channel

$$E_{\perp} = U(r_{\min}) = E\psi^2 + U(d_{ach}/2). \quad (2.12)$$

We proceeded in two ways to define the axial channel radius ($d_{ach}/2$) for the axial channels we included in our calculation. We used the contour plots of the axial continuum potentials plotted in a plane perpendicular to the channels shown in Fig. 3 of the 1995 paper of Hobler [22] to read off the channel radius $d_{ach}/2$ of the $\langle 100 \rangle$, $\langle 110 \rangle$ and $\langle 111 \rangle$ axial channels in terms of the lattice constant a_{lat} . They are $0.25 a_{lat}$, $0.375 a_{lat}$, and $\sqrt{0.2^2 + 0.12^2} a_{lat} = 0.233 a_{lat}$, respectively. For the other axial channels we considered, $\langle 211 \rangle$ and $\langle 311 \rangle$, we define the channel width d_{ach} in terms of the interatomic distance d in the corresponding row as $d_{ach} = 1/\sqrt{Nd}$, where is N the atomic density. For a planar channel we replace the axial potential at the middle of the axial channel $U(d_{ach}/2)$ in Eq. 2.12 by the planar potential

at the middle of the planar channel $U_p(d_{pch}/2)$ (the channel width d_{pch} was defined after Eq. 2.6).

For axial channeling Lindhard equates the condition for channeling with the condition in Eq. 2.8 for the validity of the continuum model. Replacing the inequality in Eq. 2.8 by an equality defines an energy dependent critical distance r_c , so that channeling can happen only if the propagating ion always keeps a distance $r > r_c$. Morgan and Van Vliet [17] use 5 instead of 8 in Eq. 2.8, because this agrees better with their simulations of channeling in copper crystals. Following Hobler [22], we use here Morgan and Van Vliet's equation to define r_c , i.e.

$$U''(r_c) = \frac{5}{d^2}E. \quad (2.13)$$

With Molière's form of the potential it is not possible to solve analytically for r_c . Morgan and Van Vliet [17] gave the following approximate analytical solution for the axial channeling minimum distance of approach,

$$r_c^{MV} = (2/3)a\sqrt{\alpha} [1 - (\sqrt{\alpha}/19) + (\alpha/700)] \quad (2.14)$$

with $\alpha = (Z_1Z_2e^2d/a^2E)$. This solution is not correct at low energies (high values of α). As

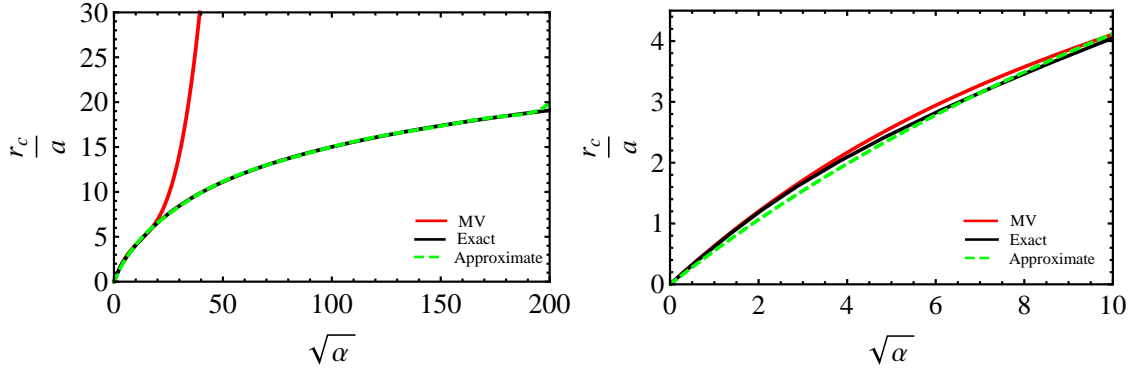


Figure 2: Comparison of the exact numerical solution (solid black) of Eq. 2.13 for the critical distance of approach $r_c(E)$ and the approximate analytic expression in Eq. 2.15 (dashed green) as a function of $\sqrt{\alpha} = \sqrt{Z_1Z_2e^2d/a^2E}$ for (a) the high $\sqrt{\alpha}$ (low energy) range, and (b) the low $\sqrt{\alpha}$ (high energy) range. The Morgan and Van Vliet approximation to $r_c(E)$ in Eq. 2.14 is also shown (solid red- labeled MV).

can be seen in Fig. 2 (and also in Figs. 8 and 13 of the 1995 paper of Hobler [22]) the steep increase in the approximate Morgan and Van Vliet solution at low energies (see the curve labeled “MV” in Fig. 2.a) is not present in the numerical solution (see the curve labeled “Exact” in Fig. 2.a) of r_c . Instead of Eq. 2.14 we use here a better approximate analytic solution obtained by fitting a degree nine polynomial to the exact solution of Eq. 2.13,

$$r_c = a [0.57305\sqrt{\alpha} - 0.0220301(\sqrt{\alpha})^2 + 0.000728889(\sqrt{\alpha})^3 - 0.0000155189(\sqrt{\alpha})^4 + 2.04162 \times 10^{-7}(\sqrt{\alpha})^5 - 1.65057 \times 10^{-9}(\sqrt{\alpha})^6 + 7.9749 \times 10^{-12}(\sqrt{\alpha})^7 - 2.11041 \times 10^{-14}(\sqrt{\alpha})^8 + 2.35121 \times 10^{-17}(\sqrt{\alpha})^9]. \quad (2.15)$$

Eq. 2.15 is valid from E of 1 keV to 29 TeV (which corresponds to values of \sqrt{a} between 180 and 0.000158). Fig. 2 shows a comparison of the exact numerical solution $r_c(E)$ of Eq. 2.8 and the approximate analytic solution Eq. 2.15 as a function of \sqrt{a} (divided by the screening distance a). The high and low \sqrt{a} range in Fig. 2.a and 2.b respectively corresponds to low and high energies. The maximum percentage error between the exact solution and the analytic approximation we use is 11.5 %.

Fig. 3 shows the critical distance of approach $r_c(E)$ in Eq. 2.15 as a function of energy of the propagating ion for several axial channels, for Si ions propagating in a Si crystal and Ge ions propagating in a Ge crystal.

Since r_c is the smallest possible minimum distance of approach to the string of a channeled propagating ion for a given energy E , i.e. $r_{\min} > r_c$, and the potential $U(r)$ decreases monotonically with increasing r , then

$$U(r_{\min}) < U(r_c). \quad (2.16)$$

Using Eq. 2.12, this can be further translated into an upper bound on E_{\perp} and thus on ψ , the angle the ion makes with the string far away from it,

$$\psi < \psi_c(E) = \sqrt{\frac{U(r_c(E)) - U(d_{\text{ach}}/2)}{E}}. \quad (2.17)$$

$\psi_c(E)$ is the critical channeling angle for the particular axial channel, i.e. it is the maximum angle the propagating ion can make with the string far away from it (in the middle of the channel) if the ion is channeled.

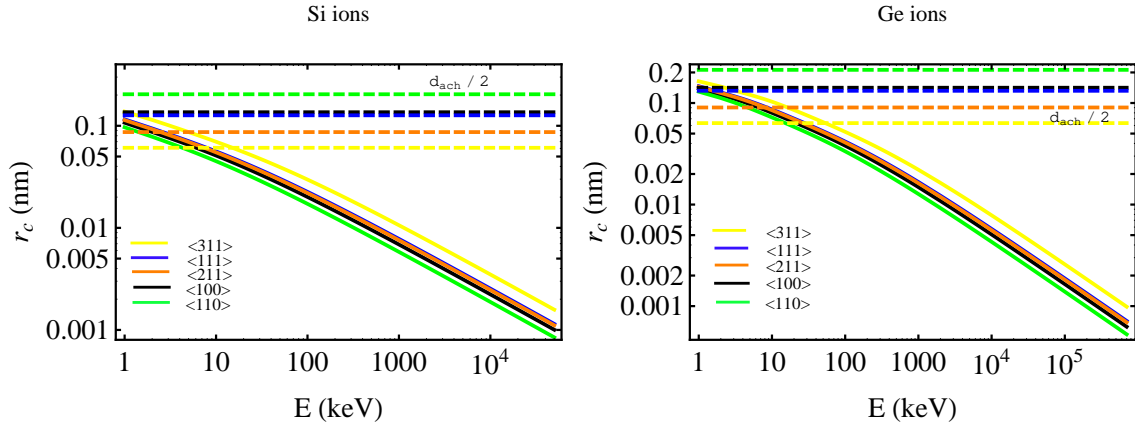


Figure 3: Critical channeling distance of approach $r_c(E)$ in Eq. 2.14 as a function of energy of the propagating ion for several axial channels, for (a) Si ions propagating in a Si crystal and (b) Ge ions propagating in a Ge crystal.

The critical distance $r_c(E)$ increases as E decreases (see Figs. 3, 5 and 7 to 13). At low enough E , $r_c(E)$ becomes close to the radius of the channel $d_{\text{ach}}/2$, and the critical angle $\psi_c(E)$ (which is the maximum angle for channeling in the middle of the channel) goes to

zero (see Figs. 7 to 10 and 14, 15). This means that there is a minimum energy below which channeling cannot happen, even for ions moving initially in the middle of the channel. This is a reflection of the fact that the range of the interaction between ion and lattice atoms increases with decreasing energy and at some point there is no position in the crystal where the ion would not be deflected at large angles. The existence of a minimum energy for channeling was found by Rozhkov and Dyuldy [28] in 1984 and later by Hobler [22] in 1996. It is clear that to compute $r_c(E)$ when it is not small with respect to the radius of the channel $d_{\text{ach}}/2$, and thus to compute the actual minimum energy for channeling, we would need to consider the effect of more than one row or plane (as done in Refs. [28] and [22]), thus our results are approximate in this case.

For planar channeling we will follow the procedure of defining a “fictitious row” introduced by Morgan and Van Vliet [17, 22]. They reduced the problem of scattering from a plane of atoms to the scattering of an equivalent row of atoms contained in a strip of width $2R$ (R is defined below) centered on the projection of the ion path onto the plane of atoms, and took the average area per atom in the plane, $1/Nd_{\text{pch}}$ to be $2R$ times the characteristic distance \bar{d} between atoms along this fictitious row, i.e.

$$\bar{d} = 1/(Nd_{\text{pch}}2R). \quad (2.18)$$

Once the width $2R$ of the fictitious row is specified, one uses the channeling condition for the continuum string model, Eq. 2.8, with the average atomic composition of the plane. For R , Morgan and Van Vliet used the impact parameter in an ion-atom collision corresponding to a deflection angle of the order of “the break-through” angle $\sqrt{U_p(0)/E}$. This is the minimum angle at which an ion of energy E must approach the plane from far away (so that the initial potential can be neglected) to overcome the potential barrier at the center of the plane at $x = 0$ (namely, so that $E_{\perp} = U_p(0)$). For small scattering angles, the deflection angle δ is related to the impact parameter, in this case R , as (see e.g. Eq. 2.1' of Lindhard [1])

$$2E\delta = -d U'(R), \quad (2.19)$$

where U' is the derivative of the axial continuum potential, and Morgan and Van Vliet define R by taking $\delta = \sqrt{U_p(0)/E}$. Using the Molière’s approximation for the potentials, Morgan and Van Vliet found the following expressions for R

$$R^{MV} = a \left(\frac{A}{2} \right) \ln \left(B Z_1 Z_2 e^2 / a \sqrt{EU_p(0)} \right) \quad (2.20)$$

which lead to the \bar{d} value

$$\bar{d}^{MV} = \left[A a N d_{\text{pch}} \ln \left(B Z_1 Z_2 e^2 / a \sqrt{EU_p(0)} \right) \right]^{-1}, \quad (2.21)$$

with coefficients $A = 1.2$ and $B = 4$. Morgan and Van Vliet [17] found discrepancies with this theoretical formula in simulations of binary collisions of 20 keV protons in a copper

crystal and adjusted the coefficients to $A = 3.6$ and $B = 2.5$. Hobler [22] used both sets of coefficients and compared them with simulations and data of B and P ions propagating in Si for energies of about 1 keV and above. Hobler concluded that the original theoretical formula was better in his case (although Hobler proposed yet another empirical relation to define \bar{d}). While Eq. 2.19 seems to provide a good condition for R , there is a channel dependent energy upper limit of applicability of its approximate analytical solution in Eq. 2.21, because the logarithm in \bar{d}^{MV} approaches zero as E approaches $(4Z_1Z_2e^2/a)^2/U_p(0)$. Close to this value of E there is an unphysical fast increase in \bar{d}^{MV} (and consequently in $x_c(E)$) that indicates the break-down of the approximate solution \bar{d}^{MV} in Eq. 2.21 (and, as shown in Fig. 13 of the 1995 paper of Hobler [22], is not found in other expressions of x_c).

We decided to keep the Morgan and Van Vliet definition for R in Eq. 2.19 and use the following approximate analytical solution obtained by fitting a degree five polynomial in $\ln y$ to the exact numerical solution of Eq. 2.19

$$R = a \left(0.716014 + 0.510922 \ln y + 0.12047(\ln y)^2 + 0.0180492(\ln y)^3 + 0.00442459(\ln y)^4 - 0.000824744(\ln y)^5 \right), \quad (2.22)$$

where $y = Z_1Z_2e^2/a\sqrt{EU_p(0)}$.

Fig. 4 shows a comparison of the exact numerical solution of Eq. 2.19 for R and its analytical approximation in Eq. 2.22 (divided by a) as a function of y . Also the approximate expression of Morgan and Van Vliet in Eq. 2.21 is shown in Fig. 4 (labeled MV). The high and low y ranges in Fig. 4.a and b respectively corresponds to low and high energies. The approximate solution is not valid at $y < 0.15$ which corresponds to $E > 50$ MeV for Si, and $E > 700$ MeV for Ge. Within its range of validity, the percentage error of the analytic approximation in Eq. 2.22 is less than 9%.

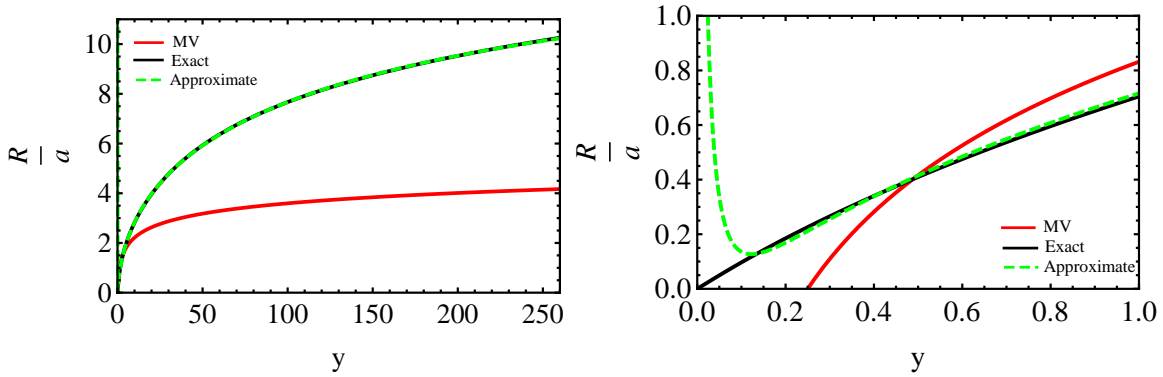


Figure 4: Comparison of the exact solution (solid black) of Eq. 2.19 for R/a and its analytical approximation in Eq. 2.22 (dashed green) as a function of $y = Z_1Z_2e^2/a\sqrt{EU_p(0)}$ for the (a) high y (low E) range and the (b) low y (high E) range. Also the Morgan and Van Vliet approximation to R/a in Eq. 2.20 is shown (solid red- labeled MV).

Let us call $\bar{r}_c(E)$ the critical distance obtained from Eq. 2.15 for the fictitious row, whose interatomic distance is \bar{d} in Eq. 2.18 in which the distance R is given in Eq. 2.22. Then, the

minimum distance of approach for planar channeling is

$$x_c(E) \equiv \bar{r}_c(E). \quad (2.23)$$

Fig. 5 shows the plot of $x_c(E)$ (obtained from using Eq. 2.22 for the fictitious string) as a function of energy for the most important planar channels, i.e. $\{100\}$, $\{110\}$, $\{111\}$, $\{210\}$ and $\{310\}$. Fig. 5 shows that we can safely extend our approximation to 50 MeV for Si ions in a Si crystal and to 700 MeV for Ge ions in Ge crystals.

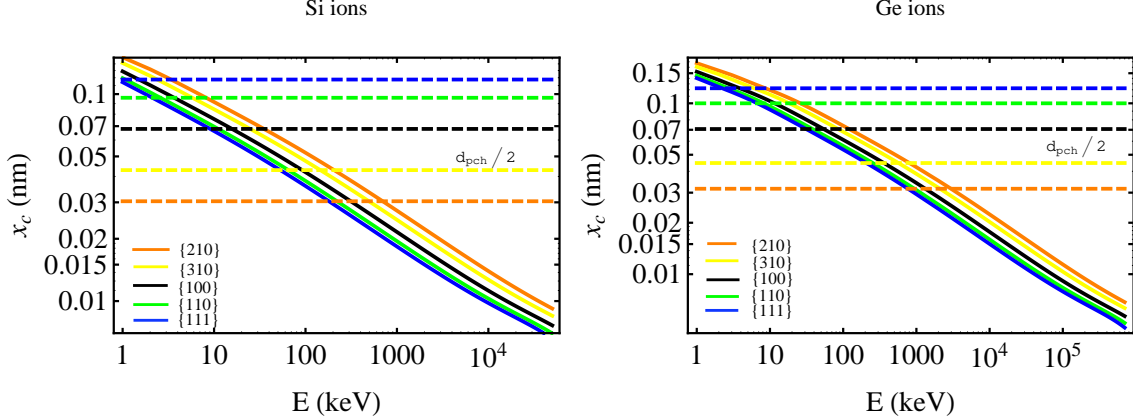


Figure 5: Critical channeling distances $x_c(E)$ in Eq. 2.23 as a function of the energy of the propagating ion for different planar channels, for (a) Si ions propagating in a Si crystal and (b) Ge ions in Ge.

Writing equations equivalent to Eqs. 2.12 and 2.16 for planar channels, namely

$$E_{\perp} = U_p(x_{\min}) = E(\psi^p)^2 + U_p(d_{pch}/2) \quad (2.24)$$

and

$$U_p(x_{\min}) < U_p(x_c(E)), \quad (2.25)$$

we obtain an equation similar to Eq. 2.17 but for the maximum planar channeling angle, the critical planar channeling angle

$$\psi_c^p(E) = \sqrt{\frac{U_p(x_c(E)) - U_p(d_{pch}/2)}{E}}. \quad (2.26)$$

For very small energies, for which $x_c(E) \geq d_{pch}/2$ no channeling is possible (the maximum distance to any plane cannot be larger than half the width of the channel separating them) and $\psi_c^p = 0$ (see Figs. 5, 7 to 10 and 14.b, 15.b). When $x_c(E)$ approaches the middle of the channel the effect of other planes should be considered, so our approximation of using the potential of only one plane is not correct in this regime.

The static lattice critical distances presented in Figs 3 and 5 (also in the left panels of Figs. 7, 8, 9 and 10) do not include thermal effects. These are important and must be taken into account. They increase the critical channeling distances and consequently decrease the critical channeling angles as the temperature increases (as clearly shown in Fig. 12 and 13).

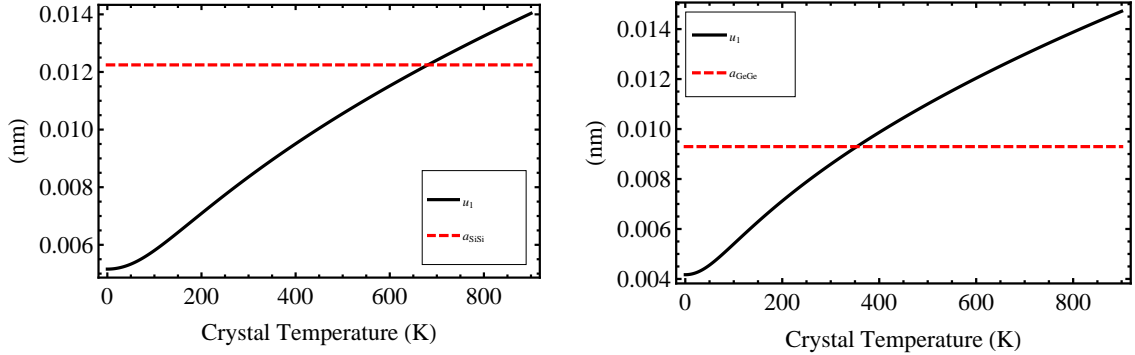


Figure 6: Temperature dependent Debye model one dimensional rms vibration amplitude $u_1(T)$ (Eq. 2.27) of the atoms in (a) a Si crystal and (b) a Ge crystal. For comparison the Thomas-Fermi screening distances for two Si atoms and two Ge atoms, a_{SiSi} and a_{GeGe} respectively are also indicated (see App. A).

2.4 Temperature dependent critical distances and angles

So far we have been considering static strings and planes, but the atoms in a crystal are actually vibrating. We use here the Debye model to take into account the zero point energy and thermal vibrations of the atoms in a crystal. The one dimensional rms vibration amplitude u_1 of the atoms in a crystal in this model is [15, 21]

$$u_1(T) = 12.1 \text{ \AA} \left[\left(\frac{\Phi(\Theta/T)}{\Theta/T} + \frac{1}{4} \right) (M\Theta)^{-1} \right]^{1/2}, \quad (2.27)$$

where the $1/4$ term accounts for the zero point energy, M is the atomic mass in amu, Θ and T are the Debye temperature and the temperature of the crystal in K, respectively, and $\Phi(x)$ is the Debye function,

$$\Phi(x) = \frac{1}{x} \int_0^x \frac{tdt}{e^t - 1}. \quad (2.28)$$

The Debye temperatures of Ge and Si are respectively $\Theta = 290$ °K and $\Theta = 490$ °K [15, 22]. The vibration amplitude u_1 as a function of the temperature T is plotted in Fig. 6 for Si and Ge crystals. At room temperature (20 °C), $u_1 = 0.00849$ nm for Ge and $u_1 = 0.00827$ nm for Si.

In principle there are modifications to the continuum potentials due to thermal effects, but we are going to take into account thermal effects in the crystal through a modification of the critical distances found originally by Morgan and Van Vliet [17] and later by Hobler [22] to provide good agreement with simulations and data. For axial channels it consists of taking the temperature corrected critical distance $r_c(T)$ to be,

$$r_c(T) = \sqrt{r_c^2(E) + [c_1 u_1(T)]^2}, \quad (2.29)$$

where the dimensionless factor c_1 in different references is a number between 1 and 2 (see e.g. Eq. 2.32 of Ref. [18] and Eq. 4.13 of the 1971 Ref. [17]).

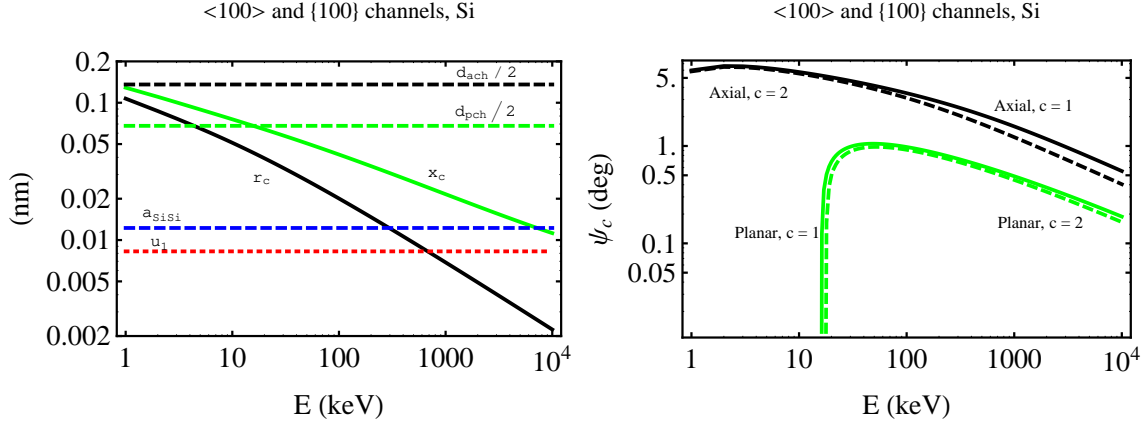


Figure 7: (a) Static critical distances of approach and Debye one dimensional rms vibration amplitude u_1 of the atoms in the crystal at 20 °C and (b) critical channeling angles at 20 °C with temperature effects computed assuming $c_1 = c_2 = c$ and $c = 1$ or $c = 2$ as indicated, as a function of the energy of propagating Si ions in the $\langle 100 \rangle$ axial (black) and $\{100\}$ planar (green/light gray) channels of a Si crystal.

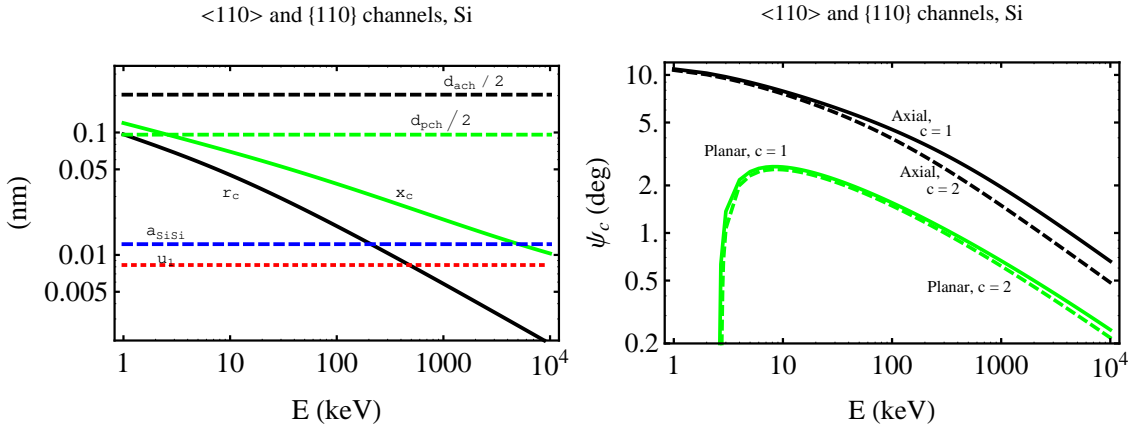


Figure 8: Same as in Fig. 7 but for the $\langle 110 \rangle$ axial and $\{110\}$ planar channels of a Si crystal.

For planar channels the situation is more complicated, because some references give a linear and others a quadratic relation between $x_c(T)$ and u_1 . Following Hobler [22] we use an equation similar to that for axial channels, namely

$$x_c(T) = \sqrt{x_c^2(E) + [c_2 u_1(T)]^2}, \quad (2.30)$$

where again c_2 is a number between 1 and 2 (for example Barret [23] finds $c_2 = 1.6$ at high energies, and Hobler [22] uses $c_2 = 2$). We will mostly use $c_1 = c_2 = 1$ in the following, to try to produce upper bounds on the channeling fractions.

Using the temperature corrected critical distances of approach $r_c(T)$ and $x_c(T)$ (Eqs. 2.29 and 2.30) instead of the static lattice critical distances r_c and x_c (Eqs. 2.15 and 2.23), in the

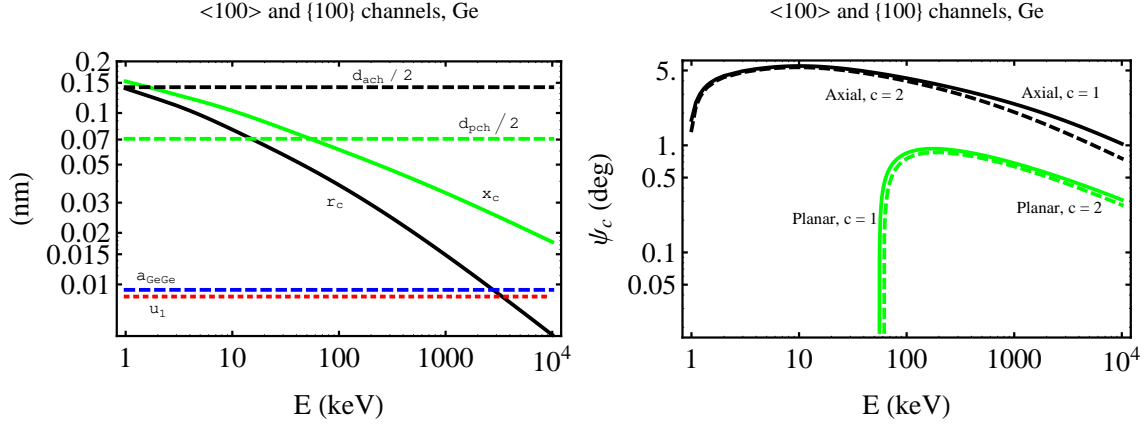


Figure 9: Same as in Fig. 7 but for Ge ions propagating in the $\langle 100 \rangle$ axial (black) and $\{100\}$ planar (green/light gray) channels of a Ge crystal.

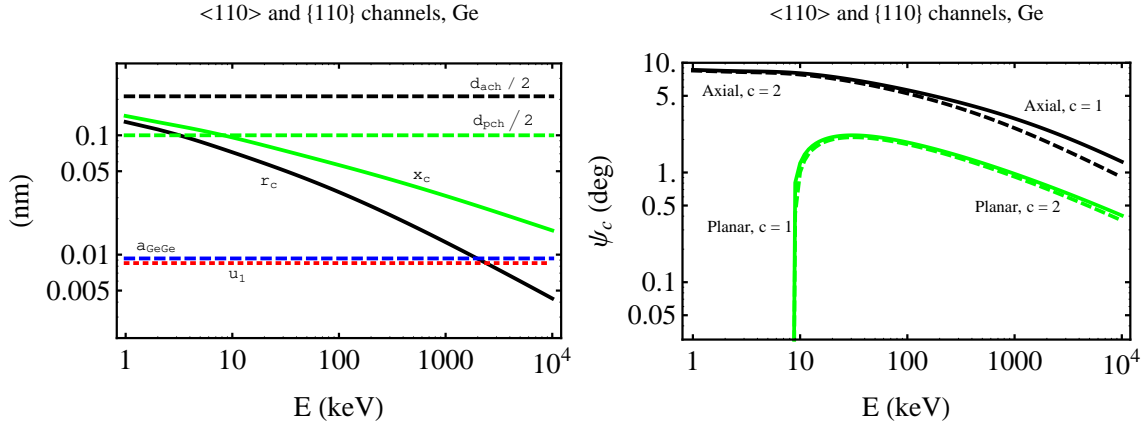


Figure 10: Same as in Fig. 9 but for the $\langle 110 \rangle$ axial and $\{110\}$ planar channels.

definition of critical angles, Eqs. 2.17 and 2.26, we obtain the temperature corrected critical axial and planar angles, examples of which are shown in the right panels of Figs. 7 to 10 ($c_1 = c_2 = c$ and $c = 1$ or $c = 2$ at room temperature).

As shown in Fig. 11, with this formalism and using $c_1 = c_2 = 2$ we fit relatively well the critical angles measured at room temperature for B and P ions in a Si crystal (shown in green, or gray if color not available) in several channels, for energies between 20 keV and 600 keV that Hobler [22] extracted from thermal wave measurements.

Figs. 12 and 13 show clearly the temperature effects in the critical distances and angles for a specific channel, the $\langle 100 \rangle$ axial channel of a Si crystal and for a propagating Si ion. At small energies the static critical distance of approach is much larger than the vibration amplitude, so temperature corrections are not important. For small enough energies the critical distance becomes larger than the radius of the channel indicating that nowhere in the channel an ion can be far enough from the row of lattice atoms for channeling to take place

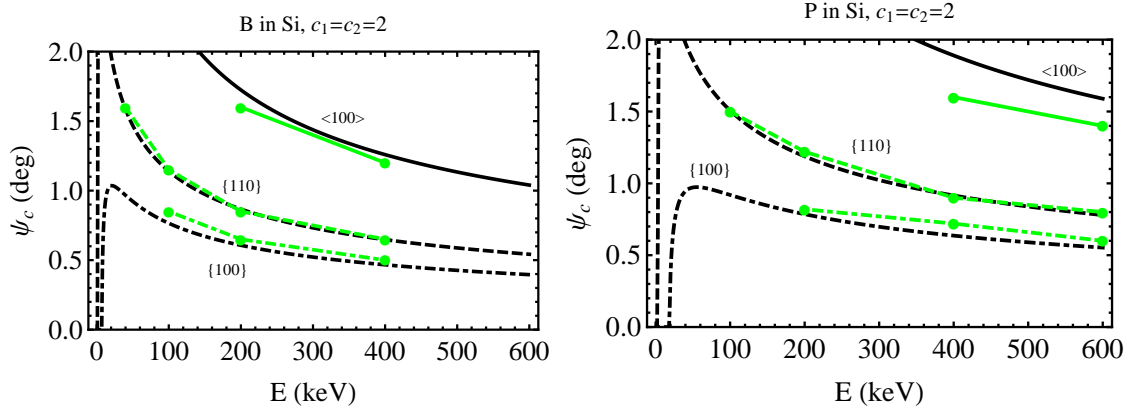


Figure 11: Comparison of theoretical (black lines) temperature corrected critical angles (with $c_1 = c_2 = 2$) and measured critical angles at room temperature extracted from thermal wave measurements [22] (green, or gray if color not available, dots joined by straight lines to guide the eye) as a function of the energy of (a) B ions and (b) P ions propagating in a Si crystal at $T=20$ °C, for the indicated axial and planar channels.

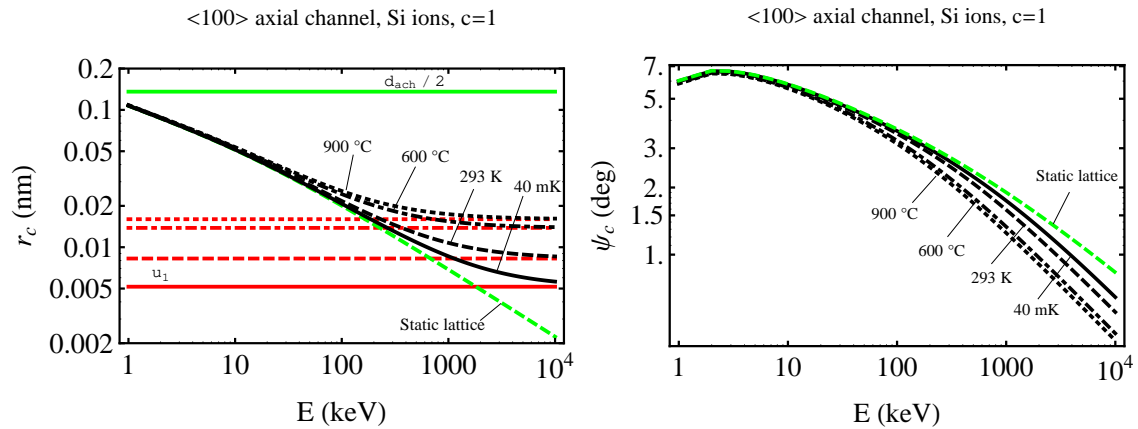


Figure 12: Static (green) and temperature corrected with $c_1 = c_2 = c = 1$ (black) (a) critical distances of approach (and $u_1(T)$ in red) and (b) the corresponding critical channeling angles as a function of the energy of propagating Si ions in $\langle 100 \rangle$ axial channels of a Si crystal.

(thus the critical channeling angle is zero). The exact calculation of the energy at which this happens would require considering the effect of more than a single row of atoms (which we do not do here) thus our results at these low energies are only approximate. As the energy increases, the static critical distance of approach decreases and when it becomes small with respect to the vibration amplitude u_1 , the temperature corrected critical distance becomes equal to $(c_1 u_1)$ which is larger for larger values of c_1 . When $u_1(T)$ becomes important in determining the critical distance, this becomes larger, and therefore the critical channeling angle become smaller, for higher temperatures.

Figs. 14 and 15 show how the critical channeling angles change with temperature for four

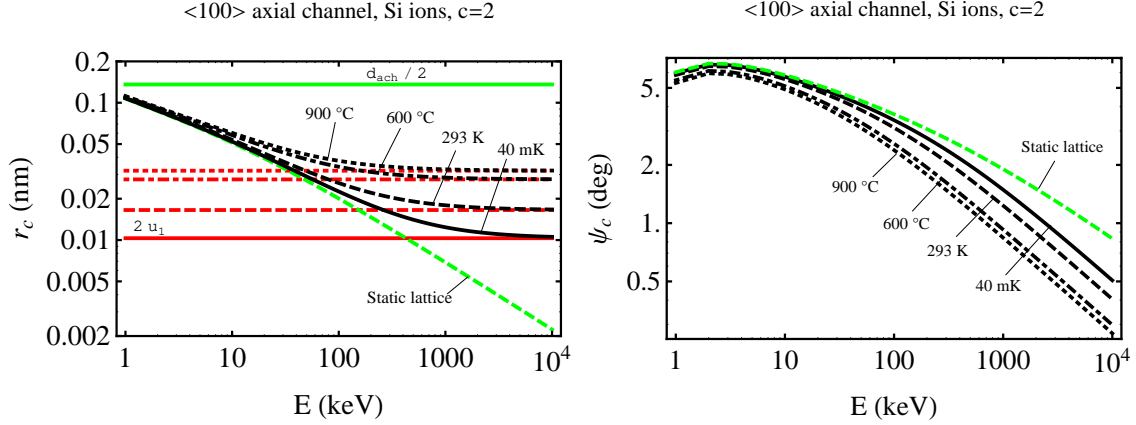


Figure 13: Same as Fig. 12 but using $c_1 = c_2 = c = 2$ in the temperature corrected critical distances of approach.

particular channels, the $\langle 110 \rangle$ and $\langle 100 \rangle$ axial and the $\{110\}$ and $\{100\}$ planar channels, for Si ions in Si and Ge ions in Ge, respectively. In both cases the axial channeling angles are larger than the planar critical angles. The $\langle 110 \rangle$ and $\{111\}$ critical channeling angles are the largest among the axial and planar channels respectively. For example, at $E = 200$ keV for Si ions in Si, the channels with the largest channeling angles are (in order of decreasing channeling angles): $\langle 110 \rangle$, $\langle 100 \rangle$, $\langle 211 \rangle$, $\langle 111 \rangle$, $\{111\}$, $\langle 311 \rangle$, $\{110\}$, $\{100\}$, $\{310\}$, and $\{210\}$. We can clearly see that the critical angles become zero at low enough energies

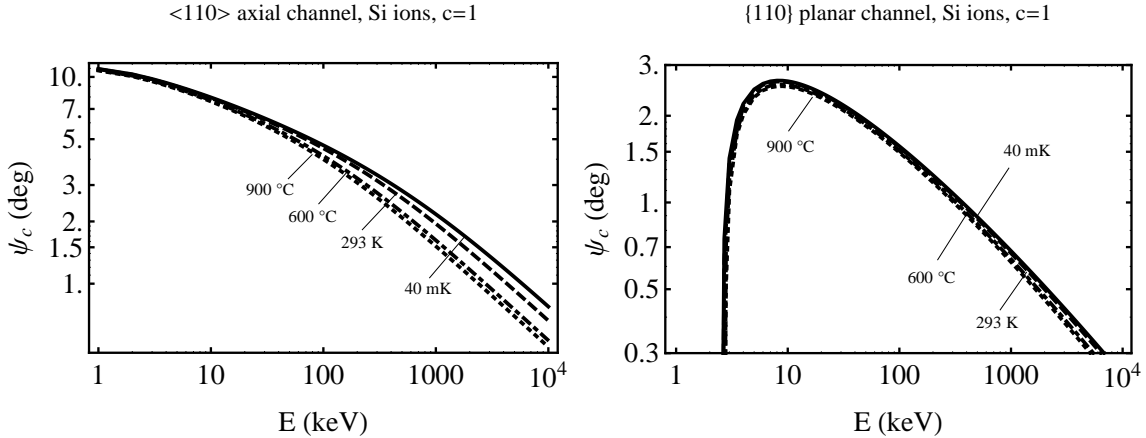


Figure 14: Temperature corrected critical channeling angles for $T=40$ mK, $T=20$ °C, $T=600$ °C, and $T=900$ °C as a function of the energy of a Si ion propagating in the (a) $\langle 110 \rangle$ axial channels and (b) $\{110\}$ planar channels of Si crystal.

(for which the critical distance of approach needed for channeling should be larger than the radius of the channel) indicating the range of energies for which no channeling is possible.

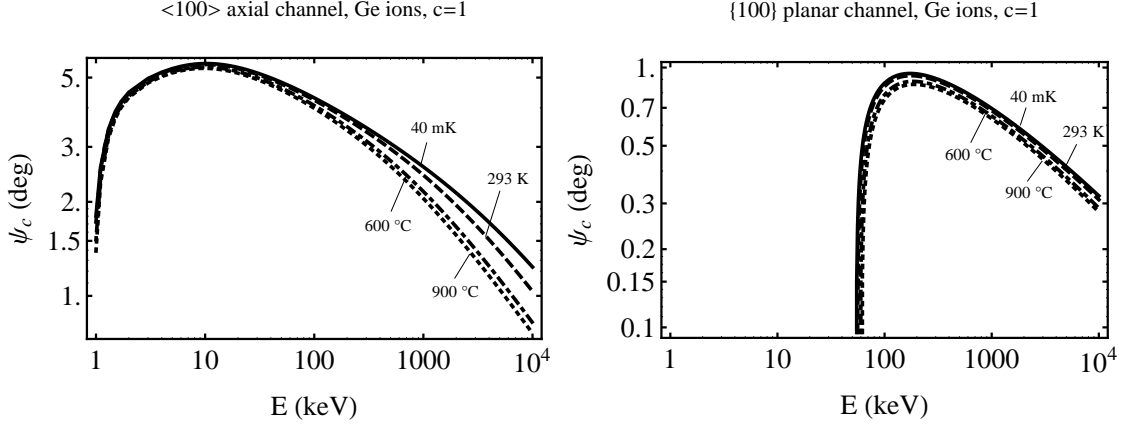


Figure 15: Same as Fig. 14 but for a Ge ion propagating in the (a) $\langle 100 \rangle$ axial channels and (b) $\{100\}$ planar channels of a Ge crystal.

3. Channeling of recoiling lattice nuclei

The channeling of ions in a crystal depends not only on the angle their initial trajectory makes with rows or planes, but also on their initial position. The nuclei recoiling after an interaction with a WIMP start initially from lattice sites (or very close to them), thus blocking effects are important. In fact, as argued originally by Lindhard [1], in a perfect lattice and in the absence of energy-loss processes the probability of a particle starting from a lattice site to be channeled would be zero. This is what Lindhard called the “*Rule of Reversibility.*” However, any departure of the actual lattice from a perfect lattice, for example due to vibrations of the atoms in the lattice, violates the conditions of this argument and allows for some of the recoiling lattice nuclei to be channeled. Lattice vibrations are more important at high temperatures and they have two opposite effects on channeling fractions: the probability of finding the atom which collides with a dark matter particle further out of its equilibrium position increases with increasing temperature thus channeling fractions increase, but the range of angles the trajectory of the propagating ion must make with the direction of the channel decreases with increasing temperature, which decreases the channeling fraction.

We now estimate the channeling fraction using the formalism presented so far.

3.1 Channeling fraction for each channel

As in Ref. [14] we use a Gaussian function for the probability distribution $g(r)$ for the perpendicular distance r to the row at which the atom that collides with a WIMP is located at the moment of the collision due to thermal vibrations in the crystal

$$g(r) = \frac{r}{u_1^2} \exp(-r^2/2u_1^2). \quad (3.1)$$

The one dimensional vibration amplitude u_1 is given in Eq. 2.27. As explained in detail in Ref. [14], the channeled fraction $\chi_{\text{axial}}(E, \hat{\mathbf{q}})$ of nuclei with recoil energy E moving initially

in the direction $\hat{\mathbf{q}}$ making an angle ϕ with respect to an atomic row is given by the fraction of nuclei which can be found at a distance r larger than a minimum distance $r_{i,\min}$ from the row at the moment of collision, determined by the critical distance of approach

$$\chi_{\text{axial}}(E, \phi) = \int_{r_{i,\min}}^{\infty} dr g(r) = \exp(-r_{i,\min}^2/2u_1^2). \quad (3.2)$$

It can easily be seen using Eqs. 2.10, 2.11, 2.12 and 2.16 that, because $U(r_i + d \tan \phi) \geq U(r_c)$, if $\phi > \psi_c$ no channeling can occur and $\chi_{\text{axial}}(E, \phi) = 0$.

Using the condition

$$E \sin^2 \phi + U(r_i + d \tan \phi) = U(r_{\min}) < U(r_c(E)), \quad (3.3)$$

that implies the equality for the minimum initial distance $r_{i,\min}$,

$$U(r_{i,\min} + d \tan \phi) = U(r_c(E)) - E \sin^2 \phi, \quad (3.4)$$

in Ref. [14] we derived the following analytic expression for $r_{i,\min}$ from Lindhard's approximation to the potential:

$$r_{i,\min}(E, \phi) = \frac{Ca}{\sqrt{\left(1 + \frac{C^2 a^2}{r_c^2}\right) \exp(-2 \sin^2 \phi / \psi_1^2) - 1}} - d \tan \phi, \quad (3.5)$$

where C is a constant, which was found experimentally to be $C \simeq \sqrt{3}$ [1]. We use here this equation because it is not possible to find a similar analytic expression using Molière's approximation to the potential (although following Hobler we use Molière's approximation to obtain the critical distances and angles). $r_{i,\min}$ is a function of the temperature too, through $r_c(T)$. Notice that a small change in the critical distance $r_c(T)$ and thus in $r_{i,\min}$ is exponentially magnified in the channeling fraction χ_{axial} (Eq. 3.2). This constitutes the most important difficulty to evaluate channeling fractions. The same happens for planar channels.

For a planar channel, the Gaussian thermal distribution for the planar potential is one-dimensional (the relevant vibrations occurring perpendicularly to the plane),

$$g(x) = (2\pi u_1^2)^{-1/2} \exp(-x^2/2u_1^2). \quad (3.6)$$

This is normalized to be 1 for $-\infty < x < +\infty$. In our calculations we only consider positive values of x , $0 < x < +\infty$, for each plane, thus we multiply $g(x)$ by a factor of 2 to find the fraction of channeled nuclei for a planar channel,

$$\chi_{\text{planar}}(E, \phi) = \int_{x_{i,\min}}^{\infty} 2 g(x) dx = \frac{2}{\sqrt{\pi}} \int_{x_{i,\min}}^{\infty} \frac{\exp(-x^2/2u_1^2)}{\sqrt{2}u_1} dx = \text{erfc}\left(\frac{x_{i,\min}}{\sqrt{2}u_1}\right),$$

where the minimum initial distance (derived in Ref. [14] using Lindhard's planar potential) is

$$x_{i,\min}(E, \phi) = \frac{(a/2) \left\{ C^2 - \left[\sqrt{(x_c^2/a^2) + C^2} - (x_c/a) - (\sin^2 \phi / \psi_a^2) \right]^2 \right\}}{\left[\sqrt{(x_c^2/a^2) + C^2} - (x_c/a) - (\sin^2 \phi / \psi_a^2) \right]} - d_p \tan \phi. \quad (3.7)$$

Here ϕ is the angle $\hat{\mathbf{q}}$ makes with the plane, defined as the complementary angle to the angle between $\hat{\mathbf{q}}$ and the normal to the plane, or as the smallest angle between $\hat{\mathbf{q}}$ and vectors lying on the plane. Also in this case, $\chi_{\text{planar}}(E, \phi) = 0$ if $\phi > \psi_c^p$. Note that $x_{i,\text{min}}$ is also a function of the temperature through its dependence on $x_c(T)$.

Using either Eq. 3.2 or Eq. 3.7, for an axial and a planar channel respectively, we define channeling fraction χ_k for each channel k , which depends on the initial energy E , initial angle ϕ and temperature T . Then we will sum over all channels and angles to obtain the total channeling fraction as function of E and T .

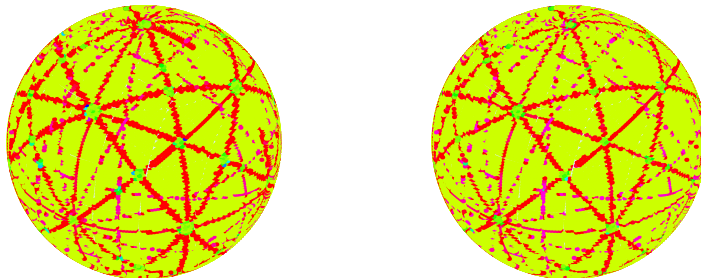


Figure 16: Geometric channeling fraction $\chi_{\text{rec}}(E, \hat{\mathbf{q}})$ including 74 channels (Eq. 3.8) for each direction $\hat{\mathbf{q}}$ plotted using the HEALPix pixelization of a sphere, for (a) a 200 keV Si ion recoil in a Si crystal, and (b) a 1 MeV Ge ion recoil in a Ge crystal, at 20 °C. Temperature effects in the lattice were included with $c_1 = c_2 = 1$. The light green, light blue, dark blue, pink, red, and yellow colors indicate a channeling fraction of 0.5, 0.013, 7.5×10^{-4} , 4×10^{-5} , 10^{-5} and zero, respectively.

3.2 Total geometric channeling fraction

The geometric channeling fraction is the fraction of recoiling ions that propagate in the 1st, or 2nd, or ... or 74th channel. Here “geometric” refers to assuming that the distribution of recoil directions is isotropic. In reality, in a dark matter direct detection experiment, the distribution of recoil directions is expected to be peaked in the direction of the average WIMP flow. Here we examine this geometrical channeling fraction, and postpone the case of a WIMP wind to another paper [30].

We include in our calculation only the most important channels, the same considered by Hobler [22]. These are the $\langle 100 \rangle$, $\langle 110 \rangle$, $\langle 111 \rangle$, $\langle 211 \rangle$ and $\langle 311 \rangle$ axial channels and the $\{100\}$, $\{110\}$, $\{111\}$, $\{210\}$ and $\{310\}$ planar channels. These constitute a total of 74 channels, as explained in Appendix B.

The probability $\chi_{\text{rec}}(E, \hat{\mathbf{q}})$ that an ion with initial energy E is channeled in a given direction $\hat{\mathbf{q}}$ is the probability that the recoiling ion enters any of the available channels, i.e.

$$\chi_{\text{rec}}(E, \hat{\mathbf{q}}) = P(A_1 \text{ or } A_2 \text{ or } \dots \text{ or } A_{74}). \quad (3.8)$$

We compute this probability in the same way we did in Ref. [14], using a recursion of the addition rule in probability theory and treating channeling along different channels as independent (see in Appendix C that this is a good approximation).

Fig. 16 shows the channeling probability $\chi_{\text{rec}}(E, \hat{\mathbf{q}})$ in Eq. 3.8 for a 200 keV recoiling Si ion in a Si crystal and a 1 MeV Ge ion recoil in a Ge crystal, at 20 °C. Temperature effects were included with $c_1 = c_2 = 1$. The probability is computed for each direction and plotted using the HEALPix pixelization of a sphere. The light green, light blue, dark blue, pink, red, and yellow colors indicate a channeling probability of 0.5, 0.013, 7.5×10^{-4} , 4×10^{-5} , 10^{-5} and zero, respectively.

To obtain the geometric total channeling fraction, we average the channeling probability $\chi_{\text{rec}}(E, \hat{\mathbf{q}})$ over the directions $\hat{\mathbf{q}}$, assuming an isotropic distribution of the initial recoiling directions $\hat{\mathbf{q}}$,

$$P_{\text{rec}}(E) = \frac{1}{4\pi} \int \chi_{\text{rec}}(E, \hat{\mathbf{q}}) d\Omega_{\hat{\mathbf{q}}}. \quad (3.9)$$

This integral is computed using HEALPix [29] (see Appendix B of Ref. [14] for a complete explanation).

Our results for the geometric total channeling fraction for Si ions in a Si crystal and Ge ions in a Ge crystal are shown in Figs. 17, 18 and 19 for three different assumptions for the effect of thermal vibrations in the lattice, which depend on the values of the parameters c_1 and c_2 used in the temperature corrected critical distances of approach $r_c(T)$ and $x_c(T)$ in Eqs. 2.29 and 2.30. The unrealistic case of assuming no vibrations in the lattice (except for vibrations of the colliding atom) corresponds to taking $c_1 = c_2 = 0$ and is shown in Fig 17 for different temperatures because it provides an upper limit to the channeling fractions. In this case the channeling fractions reach a few % and they increase with temperature.

In the literature, in other materials or for other channeling ions, values of c_1 and c_2 between 1 and 2 are used. Thus, we show the $c_1 = c_2 = 1$ choice in Fig. 18 and the $c_1 = c_2 = 2$ in Fig. 19. As the values of c_1 and c_2 increase, also the minimal distances from row or planes at which propagating ions must be to be channeled increase, thus the critical channeling angles decrease, what makes the channeling fractions smaller. If the values of c_1 and c_2 found by Hobler [22] and by us (see Fig. 11) to fit measured channeling angles for B and P ions propagating in Si apply also to the propagation of Si ions in Si, then the case of $c_1 = c_2 = 2$ in Fig. 19 should be chosen and the channeling fractions would never be larger than 0.3%. With $c_1 = c_2 = 1$ the channeling fractions reach about 1% and they increase with temperature.

Please note that we have not considered the possibility of dechanneling of initially channeled ions due to imperfections in the crystal. Any mechanism of dechanneling will decrease the fractions obtained here.

4. Main results and conclusions

We have studied the channeling of ions recoiling after a collision with dark matter particles

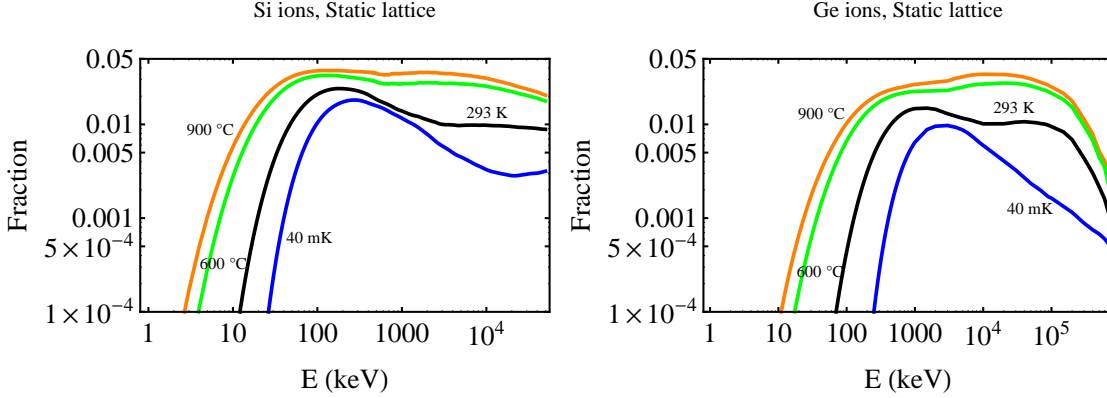


Figure 17: Channeling fractions of (a) Si and (b) Ge recoils in a Si and a Ge crystal respectively, as a function of the ion energy for temperatures $T=900$ °C (orange or medium gray), 600 °C (green or light gray), 293 K (black), and 44 mK (blue or dark gray) in the approximation of $c_1 = c_2 = 0$ (“static lattice”). This is an upper bound with respect to any non-zero values of c_1 and c_2 . Temperature effect are included in the vibrations of the colliding atom.

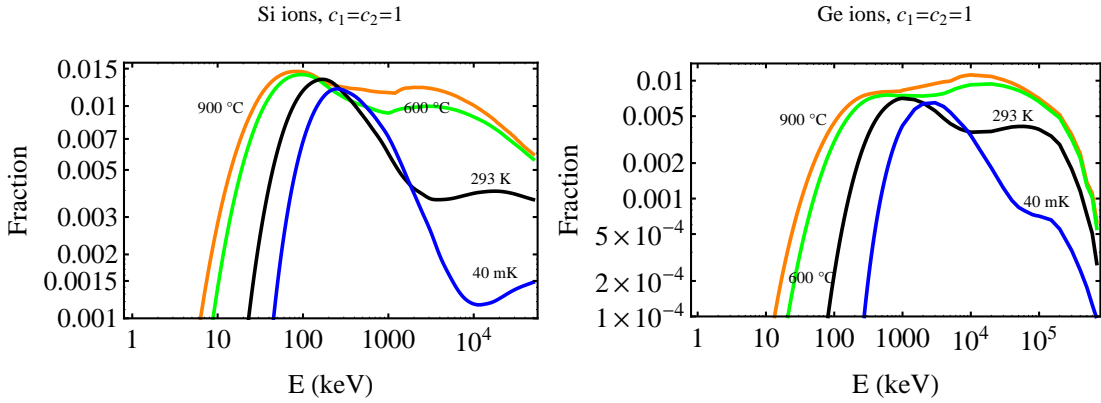


Figure 18: Same as Fig. 17 but with $c_1 = c_2 = 1$.

within Si and Ge crystals. The calculations are similar because both crystals have the same structure. Channeled ions move within the crystal along symmetry axes and planes and suffer a series of small-angle scatterings that maintain them in the open “channels” in between the rows or planes of lattice atoms and thus penetrate much further into the crystal than in other directions. In order for the scattering to happen at small enough angles, the propagating ion must not approach a row or plane closer than a critical distance r_c or x_c respectively. These are given in Eqs. 2.15 and 2.23 for a “static lattice” (i.e. a perfect lattice in which all vibrations are neglected) and by Eqs. 2.29 and 2.30 once temperature vibrations of the crystal lattice are taken into account. The temperature corrected minimum distances of approach (in Eqs. 2.29 and 2.30) depend on the one dimensional rms vibration amplitude $u_1(T)$ (Eq. 2.27), which increases with the temperature, through the coefficients c_1 and c_2 . These dimensionless coefficients are found in the literature (for different ions and/or crystals)

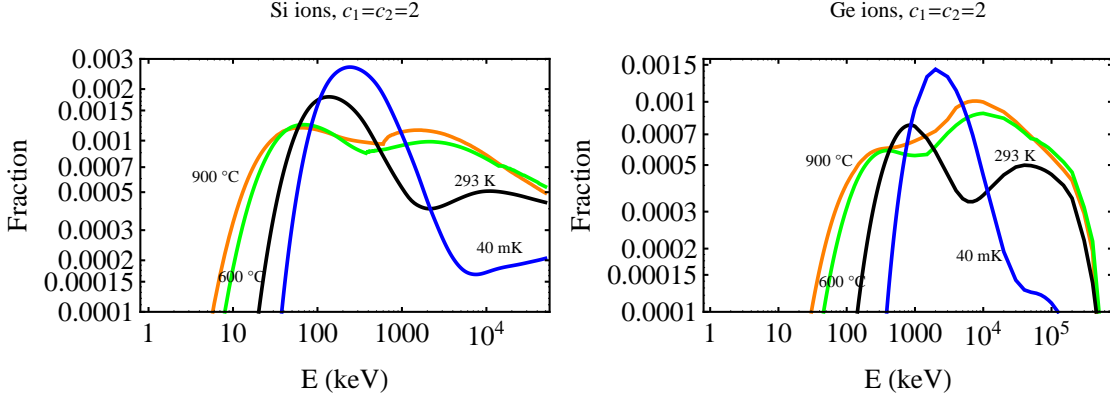


Figure 19: Same as Fig. 17 but with $c_1 = c_2 = 2$.

to take values between 1 and 2. Channeled ions must have trajectories that at large distances from the atomic rows or planes must make an angle with respect to these rows or planes smaller than a critical angle given in Eqs. 2.17 and 2.26 for axial and planar channels respectively.

The critical angles depend on the temperature through the minimum distances of approach: as these increase with increasing temperatures, the critical angles decrease, what makes the channeling fraction smaller. However, there is a second temperature effect which makes the channeling fractions larger as the temperature increases: the vibrations of the atom which collides with the dark matter particle. Thus, the channeling fraction of recoiling ions is strongly temperature dependent. Depending on which of the two competing effects is dominant, the channeling fraction may either increase or decrease as the temperature increases. Increasing the temperature of a crystal usually increases the fraction of channeled recoiling ions (see Figs. 17 and 18), but when the values of c_1 and c_2 are large (i.e. close to 2) so the critical distances increase rapidly with the temperature, the opposite may happen (see Fig. 19).

The vibrations of the atom colliding with the dark matter particle are essential to have a non-zero probability of channeling of the recoiling ion. A nucleus ejected from its lattice site by a collision with a dark matter particle is initially part of a row or plane. Thus, the recoiling nuclei start initially from lattice sites or very close to them. This means that blocking effects are important. In fact, as argued originally by Lindhard [1], in a perfect lattice and in the absence of energy-loss processes the probability of a particle starting from a lattice site to be channeled would be zero. This is what Lindhard called the “*Rule of Reversibility.*” However, vibrations of the atoms in the lattice violate the conditions of this argument and allow for some of the recoiling lattice nuclei to be channeled. The channeling fraction χ_{axial} , Eq. 3.2, or χ_{planar} , Eq. 3.7 for axial and planar channels respectively, is given by the fraction of nuclei which can be found further than a minimum distance $r_{i,\text{min}}$ or $x_{i,\text{min}}$ away from a row or plane at the moment of collision. This fraction increases as $u_1(T)$ increases. This is the effect that dominates the temperature dependence in Figs. 17 and 18, in which the geometric channeling

fractions increase with increasing temperature.

However, $r_{i,\min}$, Eq. 3.5 or $x_{i,\min}$, Eq. 3.7, increase with increasing critical distances and this decreases the channeling fraction. The increase of the critical distances with temperature is more accentuated for large values of c_1 and c_2 . This can be seen in Fig. 19, in which $c_1 = c_2 = 2$ and some channeling fractions are larger at lower temperatures.

The unrealistic case of assuming no vibrations in the lattice (except for vibrations of the colliding atoms) corresponds to taking $c_1 = c_2 = 0$ (this is what we call the “static lattice” approximation) shown in Fig. 17 for different temperatures, provides an upper limit to the channeling fractions. This is the limiting case of the possibility that c_1 and c_2 are smaller than 1, in which the channeling fractions reach a few % at energies of 100’s of keV and increase with temperature.

We show the $c_1 = c_2 = 1$ choice in Fig. 18 and the $c_1 = c_2 = 2$ in Fig. 19. If the values found by Hobler [22] and by us (see Fig. 11) to fit the measured channeling angles for B and P ions propagating in a Si crystal apply also to the propagation of Si ions in Si, then the case of $c_1 = c_2 = 2$ should be chosen and the channeling fractions would never be larger than a few 0.1%. In this case, as mentioned above, the channeling fractions at some energies are higher at lower temperatures. The $c_1 = c_2 = 1$ case, instead, leads to maximum channeling fractions of roughly 1 %, which increase with increasing temperature.

Notice that a small change in the critical distances $r_c(T)$ or $x_c(T)$ and thus in the initial minimum distances of approach $r_{i,\min}$ or $x_{i,\min}$ is exponentially magnified in the channeling fractions χ_{axial} , Eq. 3.2, or χ_{planar} , Eq. 3.7. This constitutes the most important difficulty to evaluate channeling fractions in the models we use.

Notice too that we have not considered any mechanism of dechanneling of the channeled ions (due to irregularities in the crystals, for example) which would decrease the channeling fractions.

Acknowledgments

N.B. and G.G. were supported in part by the US Department of Energy Grant DE-FG03-91ER40662, Task C. P.G. was supported in part by the NFS grant PHY-0756962 at the University of Utah. We would like to thank S. Nussinov and F. Avignone for several important discussions about their work, and to J. U Andersen, D. S. Gemmell, D. V. Morgan, G. Hobler, and Kai Nordlund for some exchange of information.

A. Penetration length of channeled ions

Fig. 20 shows the maximum distance, $x_{\max}(E)$ a channeled ion with initial energy E propagates in a crystal channel, according to the Lindhard-Scharff [2, 3] model of electronic energy loss, for a Si ion channeled in a Si crystal and a Ge ion in a Ge crystal. This model is valid for small enough energies, $E < (M_1/2)Z_1^{4/3}v_0^2$ (where $v_0 = e^2/\hbar = 2.2 \times 10^8$ cm/sec is the Bohr’s velocity [1]. M_1 and Z_1 are the mass and charge of the propagating ion) which is $E < 24.3$

MeV for a Si ion propagating in a Si crystal and $E < 188.7$ MeV for a Ge ion propagating in a Ge crystal. In this model the energy $E(x)$ as a function of the propagated distance x and

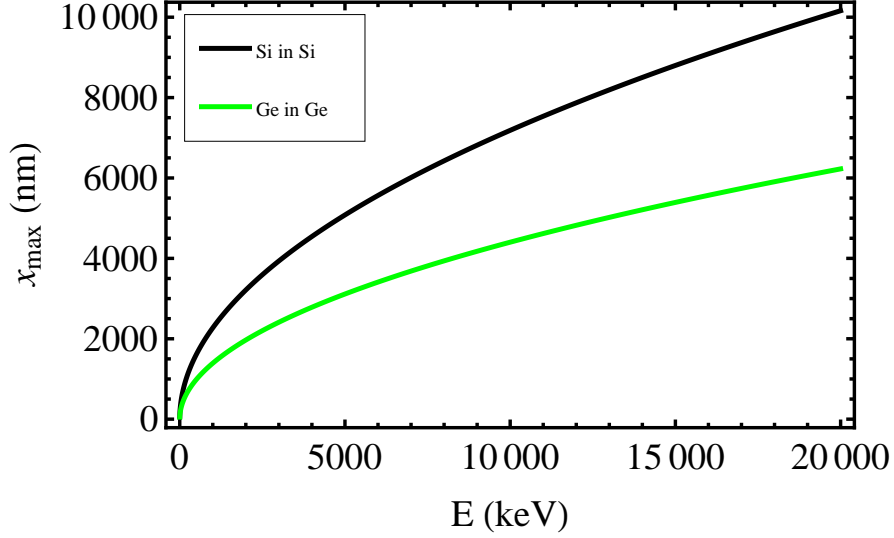


Figure 20: Maximum distance $x_{\max}(E)$ traveled by channeled Si ions in Si (black) or Ge ions in Ge (green/gray).

the initial energy E is the solution of the following energy loss equation [3]

$$-\frac{dE}{dx} = Kv, \quad (\text{A.1})$$

where $v = \sqrt{2E/M_1}$ is the ion velocity and K is the function

$$K = \frac{\xi_e 8\pi e^2 N a_0 Z_1 Z_2}{\left(Z_1^{\frac{2}{3}} + Z_2^{\frac{2}{3}}\right)^{\frac{3}{2}} v_0}. \quad (\text{A.2})$$

Here ξ_e is a dimensionless constant of the order of $Z_1^{\frac{1}{6}}$ [3], N is the number of atomic centers per unit volume, $a_0 \simeq 0.53 \text{ \AA}$ is the Bohr radius of the hydrogen atom. Explicitly, an ion with initial energy E at $x = 0$ has energy

$$E(x) = E \left(1 - \frac{x}{x_{\max}}\right)^2 \quad (\text{A.3})$$

after traveling a distance x . The range of the propagating ion is

$$x_{\max}(E) = \frac{\sqrt{2M_1 E R}}{K}. \quad (\text{A.4})$$

Fig. 20 shows that even at energies of a few keV a channeled ion interacts with hundreds of lattice atoms. The characteristic interdistance of atoms along the channels is the lattice constant, i.e. approximately 0.5 nm for Si and Ge crystals (see Appendix B).

B. Crystal structure of Si and Ge

Silicon (Si) and Germanium (Ge) crystals have a diamond cubic type lattice structure which consists of two interpenetrating face centered cubic (f.c.c.) lattices, displaced along the body diagonal of the cubic cell by one quarter of the length of the diagonal. The unit cell, shown in Fig. 21, has 8 atoms. The lattice constant, the side of the cube in Fig. 21, is $a_{\text{lat}} = 0.5431$ nm for Si and 0.5657 nm for Ge (from the Table 3.4 of Ref. [21]).

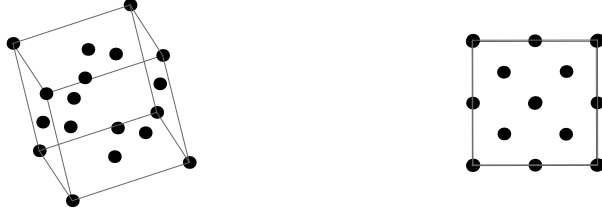


Figure 21: Unit cell of a Si or Ge crystal (a) in three dimensions, and (b) projected on a plane. The black spheres represent Si or Ge atoms.

The atomic mass and atomic number of Si and Ge are $M_{Si} = 28.09$ amu, $M_{Ge} = 72.59$ amu, $Z_{Si} = 14$ and $Z_{Ge} = 32$. The Thomas-Fermi screening distances for two Si atoms and two Ge atoms are $a_{SiSi} = 0.4685\text{\AA}(Z_{Si}^{1/2} + Z_{Si}^{1/2})^{-2/3} = 0.01225$ nm and $a_{GeGe} = 0.4685\text{\AA}(Z_{Ge}^{1/2} + Z_{Ge}^{1/2})^{-2/3} = 0.009296$ nm respectively. Once an origin of the coordinate system is fixed on a lattice point O , any position vector of a point on the crystal lattice can be written as $\mathbf{R} = n_1\mathbf{a} + n_2\mathbf{b} + n_3\mathbf{c}$ with n_1 , n_2 , and n_3 specific integer numbers. The vectors \mathbf{a} , \mathbf{b} , and \mathbf{c} are the basis vectors of the crystal lattice, and are three noncoplanar vectors joining the lattice point O to its near neighbors. For Si and Ge, the three vectors \mathbf{a} , \mathbf{b} , \mathbf{c} form a Cartesian frame and their length is $a_{\text{lat}}/4$. The integers n_1 , n_2 , and n_3 can be positive, negative, or zero. The direction of a crystal axis pointing in the direction \mathbf{R} is specified by the triplet $[n_1n_2n_3]$ written in square brackets, when n_1 , n_2 , and n_3 are positive or zero. Note that if there is a common factor in the numbers n_1 , n_2 , n_3 , this factor is removed. Moreover, negative integers are denoted with a bar over the number, e.g. -1 is denoted as $\bar{1}$ and the $-y$ axis is $[0\bar{1}0]$ direction. The plane perpendicular to the $[n_1n_2n_3]$ axis is denoted by $(n_1n_2n_3)$. For example, the plane perpendicular to the $[100]$ axis is denoted by (100) , and that perpendicular to $[101]$ by (101) . The integers n_1 , n_2 , and n_3 are called Miller indices.

In a cubic crystal, because of the symmetry of the unit cell, the directions $[100]$, $[010]$, $[001]$, $[\bar{1}00]$, $[0\bar{1}0]$ and $[00\bar{1}]$ are equivalent. All directions equivalent to the $[n_1n_2n_3]$ direction are denoted by $\langle n_1n_2n_3 \rangle$ in angular brackets. For example, $\langle 100 \rangle$ indicates all the six directions mentioned. Similarly, $\langle 211 \rangle$ and $\langle 311 \rangle$ indicate twelve different directions each.

When the unit cell has cubic symmetry, we can indicate all planes that are equivalent

to the plane (hkl) by curly brackets $\{hkl\}$. For example, the indices $\{100\}$ refer to the six planes (100) , (010) , (001) , $(\bar{1}00)$, $(0\bar{1}0)$, and $(00\bar{1})$. The negative sign over a number denotes that the plane cuts the axis on the negative side of the origin. Similarly, $\langle 210 \rangle$ and $\langle 310 \rangle$ each indicate twelve different planes.

Counting all the axes and planes we mentioned above, the total is 74.

The interatomic spacing d in atomic rows and the interplanar spacing d_{pch} (“pch” stands for “planar channel”) of atomic planes of monatomic diamond crystals, are obtained by multiplying the respective lattice constant by the following coefficients [15]:

- Rows: $\langle 100 \rangle : 1$, $\langle 110 \rangle : 1/\sqrt{2}$, $\langle 111 \rangle : 3\sqrt{3}/4$, $\langle 211 \rangle : \sqrt{6}/2$, $\langle 311 \rangle : 3\sqrt{11}/4$
- Planes: $\{100\} : 1/4$, $\{110\} : 1/2\sqrt{2}$, $\{111\} : \sqrt{3}/4$, $\{210\} : 1/(4\sqrt{5})$, $\{310\} : 1/(2\sqrt{10})$

The Debye temperatures for Si and Ge are $\Theta = 490$ K and $\Theta = 290$ K, respectively [15, 22].

C. Probability of correlated channels

In this paper, as we did in Ref. [14], we treat channeling along different channels as independent events when computing the probability $\chi_{\text{rec}}(E, \hat{\mathbf{q}})$ in Eq.3.8 that an ion with initial energy E and direction $\hat{\mathbf{q}}$ enters any of the available channels. Available channels are those whose axis or plane, respectively, form an angle with the direction $\hat{\mathbf{q}}$ smaller than the critical channeling angle for the particular channel.

In Appendix D of Ref. [14] we showed that we can obtain an upper limit to the channeling probability of overlapping channels by replacing the intersection of the complements of the integration regions in Eqs. 3.2 and 3.7 with the inscribed cylinder of radius r_{MIN} equal to the minimum of the $r_{i,\text{min}}$ or $x_{i,\text{min}}$ among the overlapping channels. We find that the two methods give practically indistinguishable results for Si and Ge (as we did in Ref. [14] for NaI), as clearly shown in Fig. 22 for some particular examples. Thus, the method we use is adequate for our purpose of providing upper bounds to the channeling fractions.

Fig. 23 shows the channeling fractions of Si ions propagating in a Si crystal and Ge ions propagating in a Ge crystal for individual channels with $c_1 = c_2 = 1$ and $T = 293$ K. The black and green (or gray) lines correspond to single axial and planar channels respectively.

Fig. 23 shows that at low E channeling is dominated by axial channels which do not overlap, so treating them as independent is strictly correct. However, at the transition energy of 1 to 10 MeV at which axial and planar channels are both equally important, and at higher energies at which planar channels dominate, the overlap of one axial and two or more planar channels, or the overlap of two or more planar channels among themselves, makes the channeling along them not necessarily uncorrelated. Still we find that considering channeling along different channels as independent is a good approximation if we are interested in providing upper bounds to the channeling fractions.

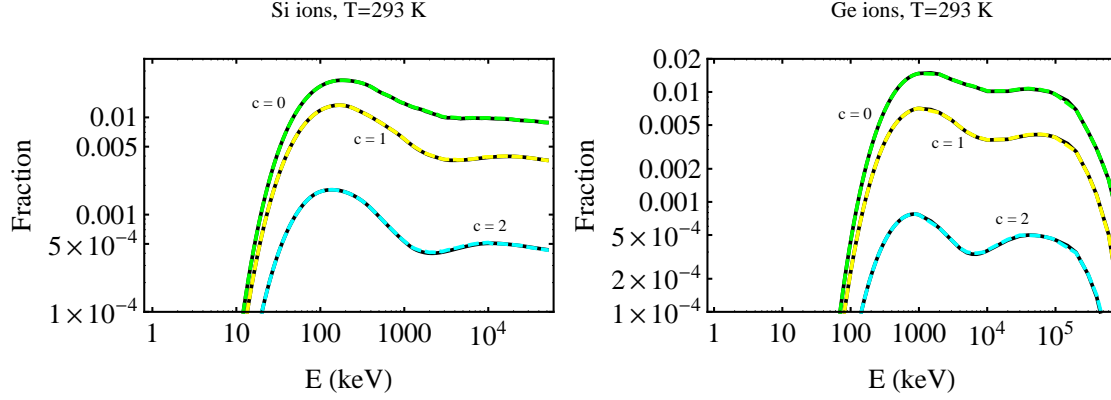


Figure 22: Maximum channeling fractions for $c_1 = c_2 = c$ and $c = 0$ (dashed green), $c = 1$ (dashed yellow) and $c = 2$ (dashed cyan) compared with the results for the same models of our method of Section 3.2 (solid black lines) or (a) Si ions propagating in a Si crystal and (b) Ge ions propagating in a Ge crystal at $T = 293$ K. Notice that the lines for the same model overlap.

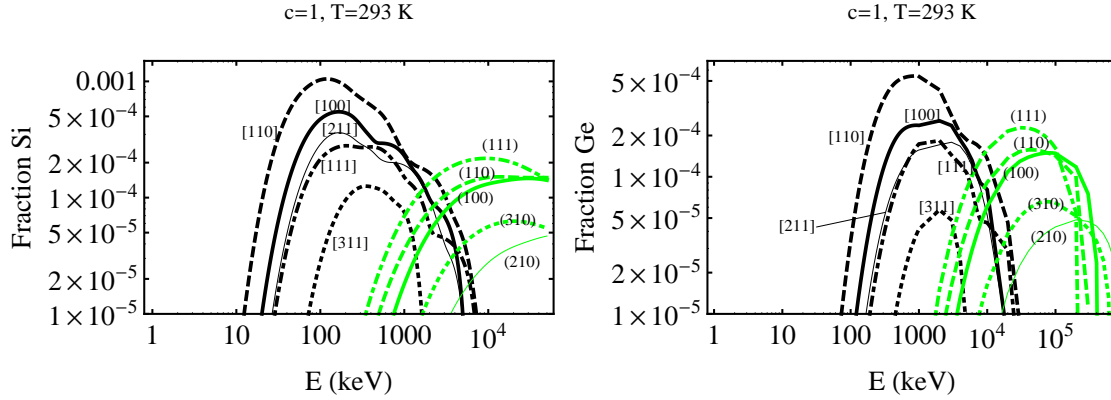


Figure 23: Channeling fractions of (a) Si ions propagating in a Si crystal and (b) Ge ions propagating in a Ge crystal for single planar (green/gray lines) and axial (black lines) channels, as function of the recoil energy E , for $T = 293$ K and $c_1 = c_2 = 1$.

References

- [1] J. Lindhard, Kongel. Dan. Vidensk. Selsk., Mat.-Fys. Medd. **34** No. 14 (1965).
- [2] J. Lindhard and M. Scharff, Phys. Rev. **124** 128 (1961).
- [3] Chapter 2 of “Ion Implantation”, by Geoffrey Dearnaley, Amsterdam, North-Holland Pub. Co.; New York, American Elsevier, 1973.
- [4] E. M. Drobyshevski, Mod. Phys. Lett. A **23** 3077 (2008) [arXiv:0706.3095 [physics.ins-det]].
- [5] R. Bernabei *et al.*, Eur. Phys. J. C **53**, 205 (2008) [arXiv:0710.0288 [astro-ph]].
- [6] F. T. Avignone, R. J. Creswick and S. Nussinov, arXiv:0807.3758 [hep-ph]; R. J. Creswick, S. Nussinov and F. T. Avignone, arXiv:1007.0214v2 [astro-ph.IM].

- [7] Z. Ahmed *et al.* (CDMS Collaboration), Phys. Rev. Lett. **102**, 011301 (2009); Z. Ahmed *et al.* (CDMS Collaboration), arXiv:0912.3592v1 [astro-ph.CO].
- [8] C. E. Aalseth *et al.* (CoGeNT Collaboration), arXiv:1002.4703v2 [astro-ph.CO].
- [9] E. Armengaud (for the Edelweiss Collaboration), Phys. Lett. B **687**, 294 (2010) [arXiv:0912.0805v1 [astro-ph.CO]].
- [10] M. Deniz *et al.* (TEXONO Collaboration), Phys. Rev. D **82**, 033004 (2010) [arXiv:1006.1947 [hep-ph]].
- [11] H. Kraus *et al.*, Nucl. Phys. B - Proceedings Supplements. **173** 168-171 (2007)
- [12] H.V. Klapdor-Kleingrothaus, Int. J. Mod. Phys. A **17** 3421-3431 (2002).
- [13] C. E. Aalseth *et al.*, Phys. Rev. D **65**, 092007 (2002) [arXiv:hep-ex/0202026].
- [14] N. Bozorgnia, G. B. Gelmini and P. Gondolo, arXiv:1006.3110 [astro-ph.CO].
- [15] D. S. Gemmell, Rev. Mod. Phys. **46** 129 (1974).
- [16] J. U. Andersen, Kongel. Dan. Vidensk. Selsk., Mat.-Fys. Medd. **36** No. 7 (1967).
- [17] D. V. Morgan and D. Van Vliet, Can. J. Phys. **46**, 503 (1963); D. V. Morgan and D. Van Vliet, Radiat. Effects and Defects in Solids, **8** 51 (1971).
- [18] D. van Vliet in “Channeling”, ed. by D. V. Morgan (Wiley, London), 37 (1973).
- [19] J.U. Andersen and L.C. Feldman, Phys. Rev. B **1**, 2063 (1970).
- [20] K. Komaki and F. Fujimoto, Phys. Stat. Sol. (a) **2** 875 (1970).
- [21] B. R. Appleton and G. Foti, “Channeling” in *Ion Beam Handbook for Material Analysis*, edited by J. W. Mayer and E. Rimini (Academic, New York), p. 67 (1977).
- [22] G. Hobler, Radiation effects and defects in solids **139** 21 (1996); G. Hobler, Nucl. Instrum. Methods Phys. Research (NIM)**B 115** 323 (1996).
- [23] J. H. Barrett, Phys. Rev. B **3** 1527 (1971).
- [24] K. Cho *et al.*, Nucl. Instrum. Meth. **B7/8** 265 (1985).
- [25] L. Rubin and J. Poate, The Industrial Physicist, June/July 2003, p.12-15.
- [26] MDRANGE, http://beam.acclab.helsinki.fi/knordlun/mdh/mdh_program.html; SRIM, <http://www.srim.org/>; TRIM, J. F. Ziegler, “Ion Implantation Technology”, Ion Implantation Technology Co. (1996); MARLOWE and UT-MARLOWE, Y. Chen *et al.*, IEEE Trans. Electron Devices, vol. 49, no. 9, 1519 (2002); Crystal-TRIM, <http://www.fzd.de/pls/rois/>; REED, K. M. Beardmore and N Gronbech-Jensen, Phys. Rev. B **60** 12610 (1999); SARIC,V. Bykov *et al.* Nucl. Instrum. Methods Phys. Research (NIM)**B 114** 371 (1996); MDRANGE, K. Nordlund, Comput. Mater. Sci. **3**, 448 (1995).
- [27] G. N. Watson, ”Theory of Bessel Functions” Cambridge U. P., Cambridge, England (1958).
- [28] V. V. Rozhkov and S. V. Dyuldyu, Pisma Zh. Tekh. Fiz. **10**, 1181 (1984) [Sov. Tech. Phys. Lett. **10**, 499 (1984)].
- [29] K. M. Górski *et al.*, ApJ **622** 759 (2005).
- [30] N. Bozorgnia, G. Gelmini and P. Gondolo, “Channeling in direct dark matter detection IV: daily modulation of the WIMP signal”, in preparation.